materials

MDPI

Review

Metastable Materials Accessed under Moderate Pressure Conditions (P ≤ 3.5 GPa) in a Piston-Cylinder Press

Javier Gainza [1], Federico Serrano-Sánchez [1], João Elias F. S. Rodrigues [1], Norbert Marcel Nemes [2], José Luis Martínez [1] and José Antonio Alonso [1,*]

[1] Instituto de Ciencia de Materiales de Madrid (ICMM), Consejo Superior de Investigaciones Científicas (CSIC), Sor Juana Inés de la Cruz 3, E-28049 Madrid, Spain; jgainza@ucm.es (J.G.); fserrano@icmm.csic.es (F.S.-S.); rodrigues.joaoelias@gmail.com (J.E.F.S.R.); martinez@icmm.csic.es (J.L.M.)

[2] Departamento de Física de Materiales, Universidad Complutense de Madrid, E-28040 Madrid, Spain; nmnemes@fis.ucm.es

* Correspondence: ja.alonso@icmm.csic.es

Abstract: In this review, we describe different families of metastable materials, some of them with relevant technological applications, which can be stabilized at moderate pressures 2–3.5 GPa in a piston-cylinder press. The synthesis of some of these systems had been previously reported under higher hydrostatic pressures (6–10 GPa), but can be accessed under milder conditions in combination with reactive precursors prepared by soft-chemistry techniques. These systems include perovskites with transition metals in unusual oxidation states (e.g., $RNiO_3$ with Ni^{3+}, R = rare earths); double perovskites such as $RCu_3Mn_4O_{12}$ with Jahn–Teller Cu^{2+} ions at A sites, pyrochlores derived from $Tl_2Mn_2O_7$ with colossal magnetoresistance, pnictide skutterudites $M_xCo_4Sb_{12}$ (M = La, Yb, Ce, Sr, K) with thermoelectric properties, or metal hydrides Mg_2MH_x (M = Fe, Co, Ni) and $AMgH_3$ (A: alkali metals) with applications in hydrogen storage. The availability of substantial amounts of sample (0.5–1.5 g) allows a complete characterization of the properties of interest, including magnetic, transport, thermoelectric properties and so on, and the structural characterization by neutron or synchrotron X-ray diffraction techniques.

Keywords: high-pressure synthesis; $RNiO_3$ perovskites; metal-insulator transitions; $CaCu_3Mn_4O_{12}$; colossal magnetoresistance; $SeNiO_3$; $SeCoO_3$; $NaMgH_3$; $Tl_2Mn_2O_7$; $CoSb_3$

Citation: Gainza, J.; Serrano-Sánchez, F.; Rodrigues, J.E.F.S.; Nemes, N.M.; Martínez, J.L.; Alonso, J.A. Metastable Materials Accessed under Moderate Pressure Conditions (P ≤ 3.5 GPa) in a Piston-Cylinder Press. *Materials* **2021**, *14*, 1946. https://doi.org/10.3390/ma14081946

Academic Editor: George Kenanakis

Received: 22 March 2021
Accepted: 9 April 2021
Published: 13 April 2021

1. Introduction

Many interesting materials (oxides, chalcogenides, pnictides, hydrides) with exceptional electronic properties are metastable under ambient conditions and require special synthesis conditions such as high pressure, or the use of strongly oxidizing or reducing conditions or, in general, the utilization of moderate treatment temperatures. Some of these metastable materials, given the difficulty of their preparation, had been little studied so far, in spite of their interesting properties. This is the case, for example, of new oxides of transition metals in unusual oxidation states (e.g., V(IV), Cr(IV), Mo(V), Fe(IV), Ni(III), Cu(III)) or intermediate valence states (such as Cu(II)-Cu(III), Mn(III)-Mn(IV), Fe(II)-Fe(III)), some of which present strong electronic correlations that are responsible for interesting properties such as the superconductivity, the metallic behaviour and the metal-to-insulator transitions or the colossal magnetoresistance phenomenon. As a brief overview, the high hydrostatic pressure favours the formation of the short and strongly covalent chemical bonds characterizing the high oxidation states; on the other hand, the high pressure applied by a reactive gas such as oxygen provides the highly oxidizing conditions necessary for the stabilization of some of the mentioned valence states. Additionally, pressure prevents the decomposition of unstable reactants at the synthesis temperature (e.g., Tl_2O_3, CrO_2); it helps to increase the coordination numbers and it favours the denser phases, in perovskite-like materials [1–4], skutterudites, pyrochlores and so on. Finally, high pressure enhances

the reaction kinetics substantially. Thus, high pressure is a good choice to prepare new compounds with a low stability or a metastable character.

In the past 20 years, our group at the Instituto de Ciencia de Materiales de Madrid (CSIC) has been dealing with the stabilization of several families of metastable materials, which have been accessed with a simple piston-cylinder hydrostatic press, under moderate pressure conditions in the 2.0–3.5 GPa range. The synthesis of some of these systems was previously described to proceed at superior pressures (6–10 GPa); in our case the combination of wet chemistry procedures to obtain reactive precursors, or the choice of the reactants, was key to succeed under moderate pressure conditions. In the following we will describe some results corresponding to the families of $RNiO_3$ perovskites (R = rare-earths), $Tl_2Mn_2O_7$ pyrochlores and derivatives, $CaCu_3Mn_4O_{12}$ double perovskites and derivatives, $M_xCo_4Sb_{12}$ skutterudites (M = alkali, alkali earth or rare earth elements), (Se,Te)MO_3 (M = Ni, Mn, Co) perovskites and $AMgH_3$ hydrides (A = alkali metals).

2. Materials and Methods

In all cases, the high-pressure reactions were carried out in a piston-cylinder Rockland Research press (Rockland Research Corporation, West Nyack, NY, USA), attaining maximum pressures of 3.5 GPa (piston of $\frac{1}{2}$") or 2 GPa (piston 3/4"). The samples were introduced in gold, platinum or niobium capsules, depending on the chemical nature of the reactants. These capsules were set in graphite cylinders acting as heaters, with Pyrex sleeves acting as pressure medium (Figure 1). The final pressure was applied in cold; the temperature was increased at 20 °C/min. Pressurization and depressurization rates were 2 GPa/h. After the heating period (20–60 min), the sample was rapidly cooled (100 °C/s) and then the pressure was slowly released. Therefore, the high-pressure products were quenched to a metastable state, where they were kinetically stable for long times. The reactants and experimental details for each system were as follows:

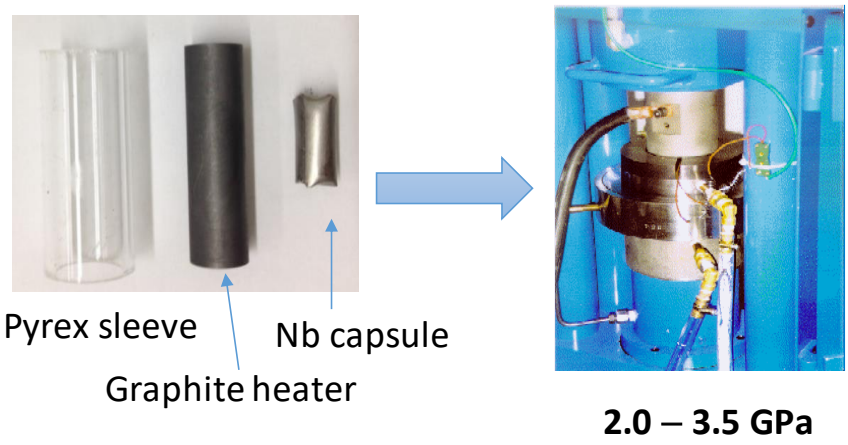

Figure 1. (**Left**): Graphite heater, Pyrex sleeve and Nb capsule (made of an Nb foil). (**Right**): view of the piston-cylinder press, including the power cable, thermocouple wiring and water cooling systems.

$RNiO_3$ perovskites. Stoichiometric mixtures of analytical grade $Ni(OH)_2$ (99%, Aldrich Chemical Company Inc., St. Louis, MO, USA) and R_2O_3 (R = rare earths) (99.9%, Alfa Aesar, Karlsruhe, Germany) were ground in an agate mortar with 30% $KClO_4$ (>99.5%, Fluka Chemika, Buchs, Switzerland), incorporated to provide an in situ high-oxygen pressure to promote the oxidation of nickel to Ni^{3+}. The precursor mixture was introduced into a gold capsule of 5 mm diameter. A hydrostatic pressure of 2 or 3.5 GPa was applied; the sample was then heated at 900 °C for 20 min, followed by quenching. The KCl resulting from the decomposition of $KClO_4$ and traces of R_2O_3 and NiO was subsequently eliminated by washing the resulting powder in a diluted HNO_3 solution (65%, J.T. Baker, Schwerte, Germany) at 60 °C. The sample was then dried at 150 °C for 1 h in air.

$RCu_3Mn_4O_{12}$ double perovskite derivatives. Stoichiometric amounts of analytical grade, R_2O_3 (R = rare earths), $Cu(NO_3)_2 \cdot 3H_2O$ and $MnCO_3$ (99.9+%, Aldrich, Steinheim, Germany) were dissolved in citric acid. For R = Ce, Pr, Tb, Th, $Ce(NO_3)_3$, Pr_6O_{13} or Tb_4O_7 or $Th(NO_3)_4 \cdot 5H_2O$ were used, respectively, instead of R_2O_3. For Fe-substituted samples, FeC_2O_4 was used as reactant. The citrate solution turned into a resin by slow evaporation and drying at 120 °C. Afterwards, all the organic materials and nitrates were eliminated by heating at 600 °C for 12 h. This precursor was mixed with $KClO_4$ (30% in weight) and thoroughly ground, sealed in a gold capsule (8 mm diameter, 10 mm length) and inserted in a cylindrical graphite heater. Hydrostatic pressure of 2 GPa and 1000 °C temperature were applied for 60 min to carry out the reaction. The in situ decomposition of $KClO_4$ provides the high O_2 pressure required to stabilize Mn^{4+} cations. Subsequently, the product was ground and washed in a dilute HNO_3 aqueous solution, in order to eliminate small amounts of unreacted CuO and dissolve KCl remaining from the decomposition of $KClO_4$; then the powder was dried in air at 150 °C for 1 h.

(Se,Te)MO_3 (M = Ni, Co, Mn) perovskites. A thoroughly ground stoichiometric mixture of TeO_2/H_2SeO_3 and $Ni(OH)_2$/CoO/MnO (99%, Alfa Aesar, Kandel, Germany) was sealed in a platinum capsule (6 mm dia.), and loaded in a cylindrical graphite heater. The reaction occurred at a pressure of 3.5 GPa at 850 °C for 1 h. After quenching to room temperature the pressure was released.

Metal hydrides, Mg_2MH_x (M = Fe, Co, Ni) and $AMgH_3$ (A: Li, Na, K). Polycrystalline samples of these nominal compositions were synthesized from stoichiometric mixtures of LiH, NaH, KH, MgH_2 and metal Fe, Co or Ni (Alfa Aesar, 99.9%, Kandel, Germany). The precursors were handled in inert atmosphere in an N_2-filled glove box, since the reactants are highly sensitive to air and moisture. The reactants were mixed and ground in a mortar and then sealed in a gold capsule (8 mm diameter, 10 mm length), and loaded in a cylindrical graphite heater. The reactions occurred at moderate conditions of 2 GPa and 775 °C for short reaction times, less than 45 min, followed by quenching to room temperature under pressure and finally releasing the pressure slowly. The gold capsule with the reaction products was opened inside the glove box, yielding dense pellets, which were ground to perform the structural characterization.

$Tl_2Mn_2O_7$ pyrochlore derivatives. $Tl_2Mn_2O_7$, $Tl_{2-x}Bi_xMn_2O_7$ (x = 0.1, 0.2), $Tl_{2-x}Cd_xMn_2O_7$ (x = 0.1, 0.2), and $Tl_2Mn_{1.8}Sb_{0.2}O_7$ pyrochlores were synthesized from Tl_2O_3, CdO/Bi_2O_3/Sb_2O_3 and MnO_2 (Alfa Aesar, 99%, Germany) powders. The oxide mixtures were sealed in an 8 mm-diameter gold capsule, and loaded in a cylindrical graphite heater. The reaction occurred in a piston-cylinder press, at a pressure of 2 GPa at 1000 °C for 1 h.

Skutterudites $M_xCo_4Sb_{12}$ (M = alkali, alkali-earth, rare-earth elements). The samples with different compositions $M_xCo_4Sb_{12}$ (M = K, Sr, Y, La, Ce, Yb, Mm (mischmetal)) have been prepared by a solid-state reaction under moderate temperature and pressure conditions. The reagents used were analytical grade KH, Sr, Y, La, Ce, Yb, Co and Sb in powder form. About 1.1 g of the starting elements was mixed according to the stoichiometric amount and sealed in a 5 mm dia. niobium capsule in an N_2-filled glove box, which was placed inside the graphite cylinder used as a heater. Reactions were carried out at a pressure of 3.5 GPa at 800 °C for 1 h. Afterwards, the products were quenched, and the pressure was released.

In all cases, the nature of the resulting powder was assessed by laboratory X-ray diffraction (XRD) in a Bruker-AXS D8 diffractometer (Bruker-AXS, Karlsruhe, Germany) (40 kV, 30 mA), with Cu Kα radiation (λ = 1.5418 Å). NPD patterns collected at the high resolution D2B neutron diffractometer of ILL-Grenoble were used for structural refinement. Although only a relatively small amount of sample was obtained from the high-pressure experiments (about 0.5 g), good quality patterns could be collected with the high-flux mode and a counting time of 4 h. A wavelength of 1.594 Å was selected from a Ge monochromator. Synchrotron X-ray diffraction (SXRD) experiments were carried out in transmission mode on the BL04-MSPD beamline of the ALBA synchrotron (Barcelona, Spain) using the highest angular resolution mode as provided by the MAD setup [5]. The samples were sealed in

0.7 mm diameter quartz capillaries that were rotating during acquisition time to increase powder averaging. The beam energy was 28 keV (λ = 0.4427 Å) or 32 keV (λ = 0.38776 Å), selected to optimize absorption. The analysis of the diffraction data was performed by the Rietveld method, using the FullProf Suite [6]. The diffraction peak shape was defined with a pseudo-Voight function; a linear interpolation between points devoid of reflections was considered as background. The final refinement included the scale factor, zero-point shift, width and asymmetry parameters, unit-cell parameters, atomic positions, and isotropic or anisotropic displacement factors. No regions were excluded from the refinements.

3. Results and Discussion

3.1. $RNiO_3$ Perovskites (R = Rare Earths)

The detailed and systematic study of the metal-to-insulator (MI) transitions in the $RNiO_3$ (R = rare earths) perovskites has been a long-standing topic, since these perovskites, containing Ni^{3+}, are paradigmatic examples of charge-transfer materials that undergo abrupt metal-insulator transitions as a function of temperature and the size of the rare-earth cation. Torrance et al. [7] interpreted such transitions in terms of the reduction and closing of the charge-transfer gap between O^{2-} and Ni^{3+} ions. The presence of trivalent nickel makes it difficult to prepare these materials, particularly with smaller lanthanide radius. Thus, the transport properties (and MI transitions) had only been reported for R between La to Eu, prepared under high-oxygen pressures of 200 bar. There are examples of Ni perovskites synthesized at elevated pressures (~6 GPa) and temperatures (1000–1200 °C) in the literature [8–10], such as $BiNiO_3$. However, the preparation of the phases for R = Y, Gd, Tb, Dy, Ho, Er, Tm, Yb, Lu, not synthesized again since the pioneering work by Démazeau in 1971 [11], was demonstrated to be possible using moderate pressures of 2 GPa. Sufficient amounts of samples were obtained to perform accurate neutron and synchrotron X-ray diffraction studies across the transitions. A charge disproportionation in $YNiO_3$ associated with the MI transition was described for the first time [12,13]. In the monoclinic $P2_1/n$ crystal structure, Ni atoms occupy two independent crystallographic sites with slightly different charge, $3 + \delta$ and $3 - \delta$, in such a way that there are alternating small and large octahedra along the 3 directions of the crystal (Figure 2).

This effect is extensive to other small rare-earth members, from R = Ho to R = Lu [14,15], for which the MI transition temperatures progressively increase as the R^{3+} size decreases (Figure 2). The access to these metastable materials made it possible to investigate a number of unexplored physical phenomena, which are mentioned hereafter: (i) High-pressure studies across the MI transitions by different techniques showed a metallization of the high-T phase for $LuNiO_3$ [16]; (ii) Mössbauer results in ^{57}Fe-doped Ni perovskites combined with neutron studies offered additional evidence of the charge disproportionation in $RNiO_3$ (R = Sm, Eu, Gd, Dy) [17–19]; (iii) Transport measurements in sintered $NdNiO_3$ yielded new features of the metallic state [20–22]; (iv) The investigation of absorbing $DyNiO_3$ in double-walled sample holders allowed the establishment of charge disproportionation and the resolution of the magnetic structure of $DyNiO_3$ [23]; (v) The observation, for the first time, of magnetic peaks by synchrotron soft X-ray resonant magnetic powder diffraction was possible in $SmNiO_3$ samples [24]; and (vi) the study of the evolution of the charge transfer between $Ni^{3+\delta}$ and $Ni^{3-\delta}$ for the whole $RNiO_3$ series was possible from X-ray absorption data [25].

More results concern (i) the study of magnetic and electronic properties of $RNiO_3$ (R = Pr, Nd, Eu, Ho and Y) from resonant X-rays [26]; (ii) the magnetism and magnetic structures of the perovskite series $NdNi_{1-x}Mn_xO_3$ from neutron powder diffraction [27]; (iii) Mössbauer results in ^{57}Fe-doped Ni perovskites combined with neutron studies offering additional evidence of the charge disproportionation in $RNiO_3$ (R = Tm and Yb) [28], and allowing us to complete the phase diagram for these materials (Figure 2); (iv) the stability of the Ni sites across the pressure-induced insulator-metal transition in $YNiO_3$, previously prepared at 2 GPa [29]; and (v) the spin-canted magnetism and decoupling of the charge and spin-orbit coupling in $NdNiO_3$ [30]. Recently, the extremely high angular resolution

of the MSPD diffractometer at ALBA synchrotron X-ray source allowed us to observe the characteristic peak splitting in the (2,2,4) and (-2,2,4) twin reflections in $SmNiO_3$ (Figure 2), thus confirming the monoclinic distortion and charge disproportionation in this perovskite with Sm^{3+} ion with a relatively large size [31].

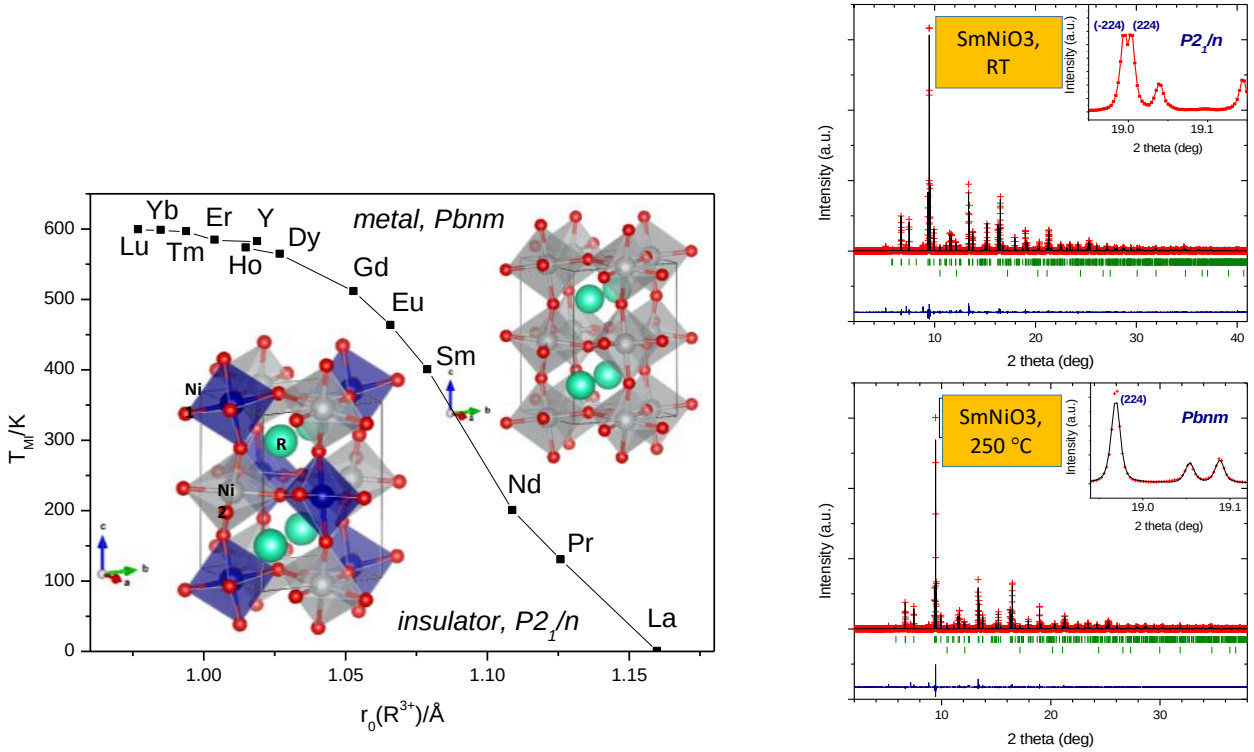

Figure 2. (**Left**): Phase diagram regarding the metal-insulator transitions experienced by $RNiO_3$ perovskites as a function of temperature and the R^{3+} ionic size. The monoclinic structure corresponding to the insulating state (space group $P2_1/n$) contains two types of crystallographically independent Ni atoms, whereas the orthorhombic structure (space group *Pbnm*) only contains one type of NiO_6 octahedron. (**Right**): Characteristic splitting of the (2,2,4)/(-2,2,4) reflections observed by synchrotron X-ray diffraction (λ = 0.4427 Å), due to the monoclinic symmetry only in the insulator regime, below the MI transition in $SmNiO_3$.

3.2. $CaCu_3Mn_4O_{12}$

Magnetoresistant (MR) materials experience an abrupt reduction in resistivity upon the application of an external magnetic field [32]. Its interest is induced, on one hand, by the wide panoply of technological applications in the field of magnetic sensors and read-head for magnetic disks. On the other hand, its study is also driven by more basic reasons, concerning the microscopic mechanisms that control these properties and, surprisingly, are related to other behaviours of the condensed matter such as the metallic state in oxides or the superconductivity.

In particular, we focus on a family of oxides that must be prepared under high-pressure conditions: the perovskites derived from $CaCu_3Mn_4O_{12}$. This oxide is among the ferrimagnetic materials that have been "rediscovered" in light of their MR properties [33,34]. This complex perovskite with a Tc = 360 K, shows a considerable MR at low field: at room temperature MR is almost saturated for magnetic fields as low as 0.03 T. Therefore, its response upon an external field is much more abrupt than for other more conventional systems. In spite of these encouraging properties, this oxide has been very little studied due to its metastable character, which requires high-pressure preparation conditions. The synthesis of this family of materials had been described, up to now, to proceed at 5–6 GPa [33,35], yet we managed to synthesize $CaCu_{2.5}Mn_{4.5}O_{12}$ at moderate pressures of 2 GPa, with comparable properties to those previously reported [36]. On the other hand, we have

checked that the replacement of Ca for La or other rare-earths in $RCu_3Mn_4O_{12}$ [37–39] has noticeable effects on the increment of T_C, besides observing a significant increase of the low-field MR, up to 3% at RT in 1 T [40].

These oxides can be considered as a 4-fold superstructure of perovskite $(ABO_3)_4$, with long-range order of R(Ca) and Cu at the A sites. The crystal structure exhibits the peculiarity of containing Cu^{2+} or Mn^{3+}, which are Jahn–Teller ions [41], at the A positions of the perovskite, in square planar coordination, as shown in Figure 3. This is due to the strong tilting of MnO_6 octahedra, defined in the *Im-3* cubic space group.

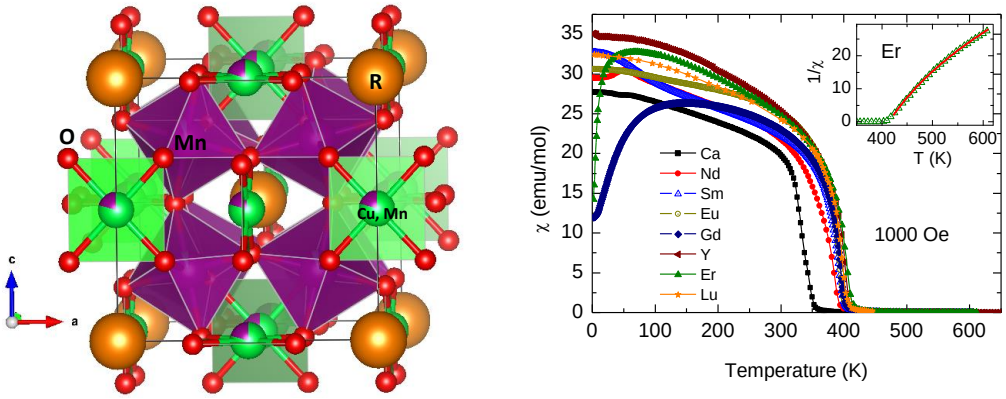

Figure 3. (**Left**): Crystal structure of $(Ca,R)_3Mn_4O_{12}$, defined in the *Im-3* space group, with the MnO_6 octahedra heavily tilted configuring a square planar oxygen coordination around Cu^{2+} (or Mn^{3+}). (**Right**): Evolution of the Curie temperature for the long-range ferrimagnetic ordering of Cu^{2+} and Mn^{4+} spins, enhanced by the decrease of the R^{3+} ionic size. The inset shows the reciprocal susceptibility above T_C for the sample with Er, characteristic of ferrimagnetic systems.

The peculiar magnetic structure of some members such as $TbCu_3Mn_4O_{12}$ has also been studied by NPD [42]. There is an interesting correlation between some structural parameters and the magnetic properties, which was discovered from neutron or synchrotron X-ray diffraction studies of all the series. By replacing Ca^{2+} with R^{3+} cations in the parent $CaCu_3Mn_4O_{12}$ oxide, there is a strong increase of the ferrimagnetic Curie temperature (T_C), shown in Figure 3, due to electron injection. The ionic radii of R^{3+} cations from La to Lu along the rare-earth series decrease, creating an internal or chemical pressure: The accompanying compression of the MnO_6 octahedral units with small rare earths brings about progressively shorter Mn-O distances and enhances the overlap between Mn and O orbitals, thus strengthening superexchange and increasing T_C by 50 K [43]. A transition from Pauli-paramagnetism to ferromagnetism was also observed in $CaCu_3(Ru_{4-x}Mn_x)O_{12}$ ($0 \leq x \leq 3$) perovskites [44], also prepared under moderate pressure conditions.

3.3. $SeMO_3$ (M = Mn, Co, Ni)

In classical ABO_3 oxides of the perovskite structure, at the A position usually an alkaline, alkaline-earth or rare-earth cation resides, with transition metals at the B sites. Much rarer are perovskite oxides containing *p-block* elements with an inert electron pair at the A positions, such as Tl^+, Sn^{2+}, Sb^{3+}, Bi^{3+}, Se^{4+} and Te^{4+}. In order to stabilize perovskitelike oxides with these rather small cations, high-pressure conditions are typically required [1]. Two important examples are $SeCuO_3$ [45] and $BiMnO_3$ [46–49]. The large structural distortion bends the superexchange Cu-O-Cu or Mn-O-Mn angles and promotes the ferromagnetic interactions, according to the Goodenough–Kanamori rules [50]. We recently prepared and studied $SeCoO_3$ [51], $SeMO_3$ (M = Ni, Mn) [52], and $TeNiO_3$ [53], which warrants the accessibility to these systems under moderate pressure conditions. There are several examples in the literature where this synthesis process has also been proven useful, such as the $SeCo_{1-x}Mn_xO_3$ material prepared at ~4 GPa and ~1100 K for 1 h [54], and the $SeMO_3$ (M = Mn, Ni) compounds synthesized at 3.5 GPa and 1123 K [55].

In addition, the lone electron pair induces cationic shifts that favour ferroelectricity: together with their magnetism, these materials are magnetoelectric, useful for multiple-memory devices (storage of information by both electric and magnetic means) or memory elements written with electric field using its ferroelectricity but read magnetically as a ferromagnetic bit. In particular, in $TeNiO_3$ [53] the extremely distorted crystal structure shapes a trigonal-pyramidal environment for the Te, where it is effectively coordinated to three oxygen atoms at Te–O distances of 1.92 Å (Figure 4). The 3-fold oxygen coordination is remarkably anomalous in perovskite-type structures, accounting for the required stabilization of these materials under high pressure conditions.

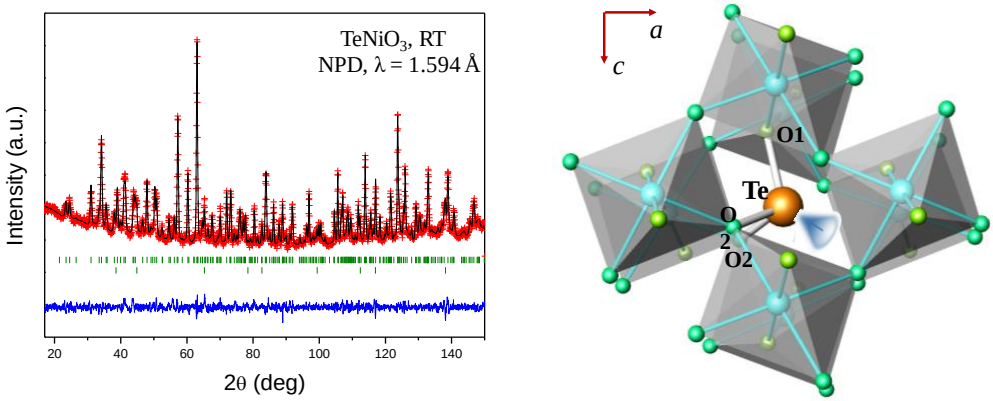

Figure 4. (**Left**): Neutron powder diffraction pattern of $TeNiO_3$ perovskite, collected at D2B diffractometer (ILL-Grenoble) from a single-batch sample obtained at 3.5 GPa. A reactive mixture of $Ni(OH)_2$ and TeO_2, contained in a sealed platinum capsule under the reaction conditions (850 °C for 2 h), was essential to succeed. (**Right**): the extremely distorted environment for Te^{4+} ions leaves room for the electron lone pair of this p element, schematically represented in this structural view, highlighting the tilting of NiO_6 octahedra.

3.4. Metal Hydrides

The utilization of hydrogen as energy vector in the coming decades has boosted the research and improvement of hydrogen storage procedures. Although the use of compressed hydrogen is the immediate choice in electrical vehicles, safety considerations in case of a crash advise delving into the research of the ideal hydrogen storage material, still undiscovered. A classic example of metal hydride with hydrogen storage properties is $LaNi_5$ and derivatives [56], able to form hydrides with composition $LaNi_5H_6$. New classes of materials composed of much lighter constituents (Li, Be, B, C, N, O, Na, Mg, Al, Si, P, S) have shown a much superior hydrogen storage capacity per weight than the conventional $LaNi_5$ materials. Especially interesting are the Mg-based hydrides, given their high mass-storage capacity; as a drawback MgH_2 is thermally stable, with decomposition temperatures above 450 °C, which prevents applications. The destabilization of MgH_2 by doping with different metals has been an active research field in recent years.

In this line, we have been successful in preparing several derivatives of the Mg_2MH_x family (M = Fe, Co, Ni) [57,58] by direct reaction between the simple hydride MgH_2 and the transition metals under high-pressure conditions, in gold capsules at 2 GPa. It is worth mentioning that Mg_2FeH_6 has one of the best H mass capacity ever described, almost 6%. Figure 5 shows the crystal structure of the novel Mg_2FeH_6 hydride, where Fe is octahedrally coordinated to hydrogen atoms. Figure 5 (right) also illustrates the cyclic hydrogen release-uptake of Mg_2NiH_4, prepared under moderate-pressure conditions.

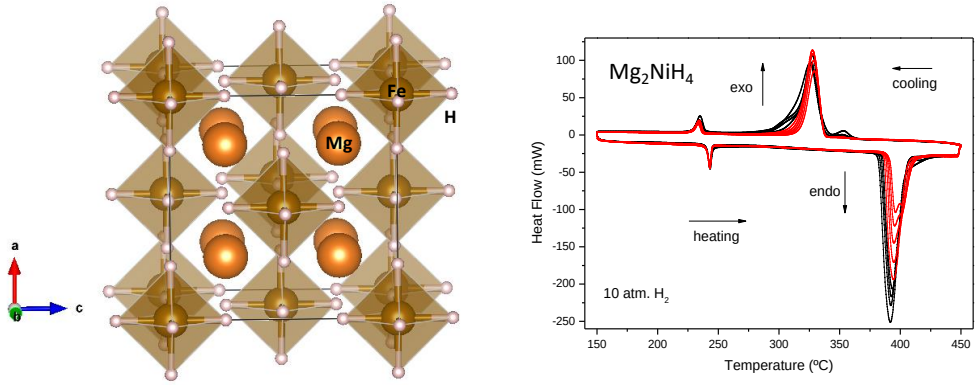

Figure 5. (**Left**): View of the crystal structure of Mg_2FeH_6, where Fe is octahedrally coordinated to 6 H atoms, while Mg is in 12-fold coordination, with Mg−H distances of 2.28 Å. (**Right**): Cyclic DSC curves of Mg_2NiH_4 in 10 bar of H_2 at 10 °C min^{-1}, showing a reduced temperature for H release with respect to MgH_2 hydride, and a moderate reversibility. 20 cycles are shown; the endothermic peaks correspond to H_2 release, and the exothermic ones to H_2 uptake.

This success in the preparative protocol has stimulated the synthesis of novel complex hydrides by direct reaction of simple hydrides under high-pressure conditions, which prevent the thermal decomposition of the reactants: we successfully prepared new hydride perovskites, of formula $Na_{1-x}Li_xH_3$, by reaction under pressure of Na(Li)H and MgH_2 [59], as well as $Na_{1-x}K_xMgH_3$ [60]. In all these compounds, the location of H atoms, the study of the tilting of the BH_6 octahedra, the presence of H vacancies and so on are also key knowledge to interpret the sorption/desorption kinetics.

Neutron diffraction techniques were powerful (and unique) tools to localize hydrogen atoms in these hydrides; Figure 6 shows the tilting of MgH_6 octahedra in $NaMgH_3$ perovskite, defined in the space group *Pbnm*, and exhibiting similar topology as the standard perovskite oxides [58]. This study demonstrated that it is not strictly necessary to study deuterated samples with neutrons, given the available flux in modern reactors or spallation sources.

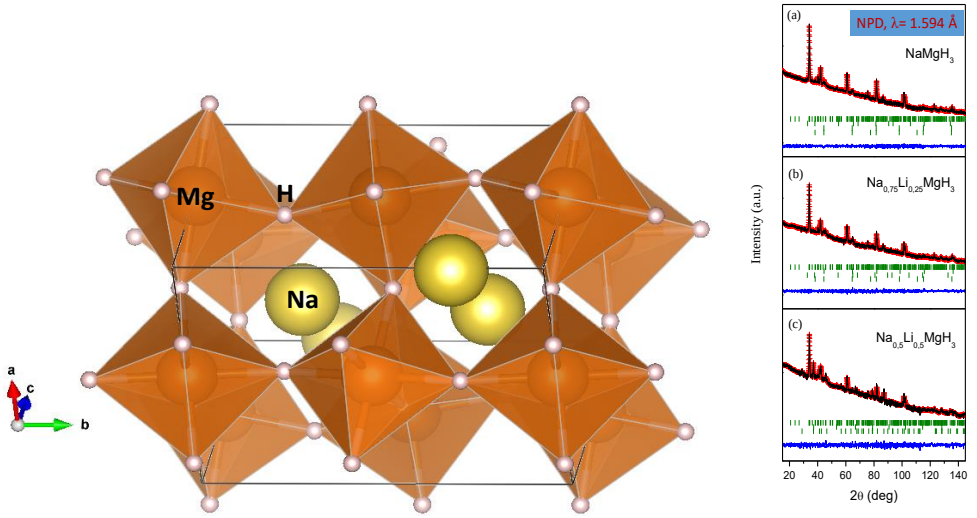

Figure 6. (**Left**): crystal structure of $NaMgH_3$, exhibiting an orthorhombic superstructure of perovskite, space group *Pbnm*, with tilted MgH_6 octahedra. (**Right**): neutron diffraction patterns for $Na_{1-x}Li_xMgH_3$, displaying in the strong background the incoherent scattering of H. (**a**): x = 0; (**b**): x = 0.25; (**c**): x = 0.5.

3.5. $Tl_2Mn_2O_7$

$Tl_2Mn_2O_7$ pyrochlore, with tetravalent valence for Mn, does not seem to follow the conventional model of Double Exchange that is formally accepted for mixed-valence perovskites [61–63]; more research demonstrates that the magnetic superexchange may be mediated by the conduction electrons [64]. $Tl_2Mn_2O_7$ is among the few metal oxides that simultaneously present ferromagnetic and metallic properties. This oxide is metastable at ambient conditions, and must be prepared under high-pressure conditions, at 2 GPa. Many efforts have been made to optimize the magnetoresistive properties of this singular material, in chemically doped derivatives. In addition, under moderate pressure conditions, diverse doped series were stabilized for the first time. The Tl sublattice of this pyrochlore has been doped with Bi, Pb and Cd, exhibiting very distinct physical properties. The Mn sublattice has been, alternatively, doped with Sb, Te and Ti [65–68]. In the Bi-doped phases, $Tl_{2-x}Bi_xMn_2O_7$, with x = 0.05, 0.1, 0.2, 0.3 [65], the presence of competitive FM and AFM interactions gives rise to a "cluster-glass-type" behaviour, and promotes the magnetoresistance (MR) by several orders of magnitude above the undoped material. Moreover, the most spectacular results were obtained for the Cd-doped pyrochlore [66], with an MR up to 10^6% at 2 K, and 20% at room temperature for magnetic field up to 0.5 T: this result has no precedents in the literature of magnetoresistive materials, and allowed proposing this material as a candidate for technological applications. Figure 7 illustrates the MR behaviour of $Tl_{2-x}Cd_xMn_2O_7$ pyrochlores, showing MR values up to 10^6 for x = 0.2.

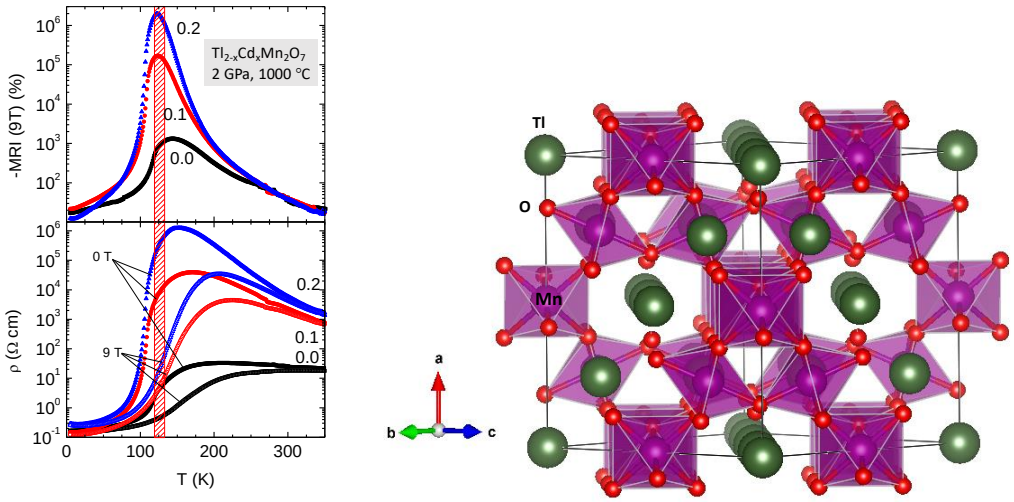

Figure 7. (**Left**): evolution of the magnetoresistance of the $Tl_{2-x}Cd_xMn_2O_7$ family, showing maxima coinciding with the insulator-to-metal transitions (lower panel) in the 120–140 K temperature range. (**Right**): Structural view of the pyrochlore structure, defined in the cubic *Fd-3m* space group.

Also extremely interesting has been the study by neutron diffraction of the structural evolution under pressure of different doped pyrochlores, depending on the chemical nature of the different bonds, Tl-O and Mn-O, for the diverse studied families [69]. Figure 7 illustrates the crystal structure of the $Tl_2Mn_2O_7$ pyrochlore, consisting of a framework of MnO_6 octahedra sharing corners with Mn-O-Mn angles of about 133°, leaving large cages where Tl ions are located.

3.6. Skutterudites $M_xCo_4Sb_{12}$ (M = Alkali, Alkali-Earth, Rare-Earth Elements)

Globally, about two-thirds of energy is dissipated as waste heat, providing an important niche for thermoelectric materials (TM). TMs can directly transform a temperature difference into electric energy [70–72]. However, a good TM must possess three antagonistic properties, hindering the design and development of novel materials: it requires a high Seebeck voltage (S, thermoelectric power), low electrical resistivity (ρ) and low thermal conductivity (κ). Most materials have a coupled thermal and electronic conductivity, since the same carriers

are involved in both mechanisms to a large extent. TMs are characterized by a Figure of Merit (ZT) defined as ($ZT = S^2T/\rho\kappa$); the best ZT is around 1–2, depending on the T range. To date, the best TMs are strongly doped semiconductors such as PbTe or Bi_2Te_3.

The possibility of preparing thermoelectric specimens under HP conditions was recently demonstrated [73–76], in particular in skutterudites. MX_3 skutterudites derive their name from Skutterud, a small town in Norway, where a mineral based on $CoAs_3$ was discovered in 1845, and their structure can host different transition metals (Fe, Co, Rh, Ir) at M position, and p-block semimetals (P, As, Sb) as X atoms [72]. A prominent feature is the existence of two relatively large voids that can be filled with additional atoms. Filled skutterudites contain lanthanide, or alkali-earth ions interstitially occupying these voids [77], with large thermal vibration parameters indicating that they can "rattle" or participate in a soft phonon mode of the crystal structure. This "ball in a cage" configuration of filled skutterudites directly determines the basic conditions for high ZT values. The effect of the atomic void fillers in oversized cages drastically reduces κ and thereby maximizes ZT [78,79]. The stabilization of such metastable compounds is possible, for example, for the parent, unfilled $CoSb_3$ pnictide, which can be successfully stabilized at 3.5 GPa, with exceptionally low thermal conductivities that were ascribed to partial Sb deficiency, the Sb vacancies acting as phonon scatterers [80]. We also stabilized $La_{1-x}CoSb_3$, with different rattling La contents, optimizing the charge carrier concentration [81], as well as Ce, Yb [82] and even with Mischmetal [83] as rattling elements (cocktail of Ce, La and other rare earths) also at 3.5 GPa. A key finding to succeed in these HP syntheses was the use of capsules made of Nb sheets, instead of the conventional Au or Pt capsules: Nb is inert with respect to Sb, and the handmade cylinders are perfectly sealed under pressure, avoiding contact with air, which would oxidize this element or the rare-earth metal fillers. There are several additional works in the literature related to the high-pressure synthesis of skutterudites, but most of them are performed at very high pressures (~6–8 GPa) [84] or in several steps [85–88]. Figure 8 shows a view of the cubic $M_xCo_4Sb_{12}$ skutterudite structure, defined in the cubic space group *Im-3*, containing strongly rotated $CoSb_6$ octahedra (Co-Sb-Co ~126°) that, in fact, is very similar to the $CaCu_3Mn_4O_{12}$ crystal structure (Figure 3), defined in the same space group, and also containing tilted MnO_6 octahedra. In the present case, the strong rotation in the space conforms square Sb_4 units (see Figure 8) that develop important role as traps for phonons, thus reducing the thermal conductivity.

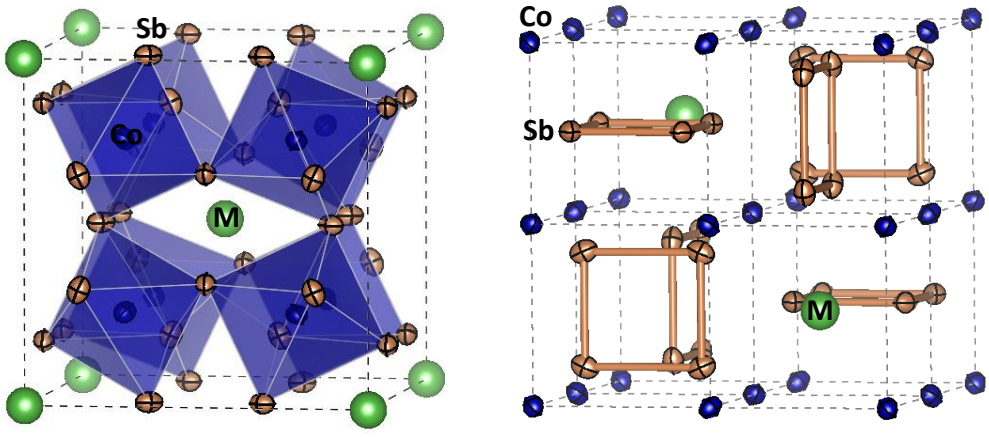

Figure 8. Two views of the skutterudite structure $M_xCo_4Sb_{12}$ (M = filler element), defined in the cubic *Im-3* space group. The strongly tilted $CoSb_6$ octahedra (**left** view) determine the presence of Sb_4 rings (**right** view), of importance in the electronic properties. The M filler elements (alkali, alkali-earths, rare-earths) occupy the large 8a voids, where the rattling diminishes the thermal conductivity.

In La-filled skutterudites, it has been additionally discovered that HP reactions favour fluctuations in the filling fraction, leading to glas-slike ultralow thermal conductivity in caged skutterudites [81]. This is in line with recent discoveries by ab initio calculations and synthesis of multiscale filling-fraction fluctuation in the RFe_4Sb_{12} system [89]. HP

brings about the separation into phases higher and lower La filler contents, leading to multiscale strain field fluctuations. The filling fraction fluctuation reduces the lattice thermal conductivity, via strain-field scattering of high-energy phonons. This strategy of favouring the uneven filling factor under HP conditions has been extended to other elements, such as K, Sr, Y and more [90].

4. Conclusions

Moderate-pressure conditions have been demonstrated to be a powerful tool for the stabilization of metastable materials with technological applications, sometimes in combination with a pertinent choice of the reactants or by elaborating suitable precursors by wet-chemistry procedures. Systems as different as transition-metal oxides in unusual oxidation states, metal pnictides or hydrides can be accessed in substantial amounts enabling a complete characterization. Besides favouring the short bonding distances of high oxidation states in densely packed structures such as perovskites, the reactions occur in laboratory-made sealed capsules avoiding the oxidation (e.g., Sb), or volatilization (e.g., SeO_2), or decomposition (e.g., NaH, MgH_2) of certain reactants, making it possible for the desired reactions in short times and controlled atmospheres (e.g., high O_2 pressure). Those findings are to be applied in novel metastable systems as upcoming research directions: Some oxides with unusual oxidation states (e.g., Fe^{4+}, in (Ca,Sr)FeO_3 derivatives), and novel pnictides and chalcogenides such as SnSe derivatives and MM'_2S_4 (M, M′ = transition metals) thiospinels, accessible under moderate-pressure conditions, are to be exploited in the near future.

Author Contributions: Conceptualization, J.A.A., N.M.N. and J.L.M.; methodology, J.G., F.S.-S. and J.E.F.S.R.; writing—original draft preparation, J.A.A. and J.G.; writing—review and editing, N.M.N.; funding acquisition, J.A.A., N.M.N. and J.L.M. All authors have read and agreed to the published version of the manuscript.

Funding: This research was funded by the Spanish Ministry of Science, Innovation, and Universities for funding the project number: MAT2017-84496-R.

Institutional Review Board Statement: Not applicable.

Informed Consent Statement: Not applicable.

Data Availability Statement: No new data were created or analyzed in this study. Data sharing is not applicable to this article.

Acknowledgments: J.G. thanks MICINN for granting the contract: PRE2018-083398.

Conflicts of Interest: The authors declare no conflict of interest.

References

1. Goodenough, J.B.; Kafalas, J.A.; Longo, J.M. *Preparative Methods in Solid State Chemistry*; Hagenmüller, P., Ed.; Academic Press: New York, NY, USA, 1972.
2. Demazeau, G. New problems in solid-state chemistry solved by high pressure conditions: An exciting perspective for preparing new materials. *Chim. Scr.* **1988**, *28*, 21–24. [CrossRef]
3. Demazeau, G. High pressure in solid-state chemistry. *J. Phys. Condens. Matter* **2002**, *14*, 11031–11035. [CrossRef]
4. Rodgers, J.A.; Williams, A.J.; Attfield, J.P. High-pressure/High-temperature Synthesis of Transition Metal Oxide Perovskites. *Zeitschrift für Naturforschung B* **2006**, *61*, 1515–1526. [CrossRef]
5. Fauth, F.; Boer, R.; Gil-Ortiz, F.; Popescu, C.; Vallcorba, O.; Peral, I.; Fullà, D.; Benach, J.; Juanhuix, J. The crystallography stations at the Alba synchrotron. *Eur. Phys. J. Plus* **2015**, *130*, 160. [CrossRef]
6. Rodríguez-Carvajal, J. Recent advances in magnetic structure determination by neutron powder diffraction. *Phys. B Phys. Condens. Matter* **1993**, *192*, 55–69. [CrossRef]
7. Torrance, J.; Lacorre, P.; Nazzal, A.; Ansaldo, E.; Niedermayer, C. Systematic study of insulator-metal transitions in perovskites $RNiO_3$ (R = Pr, Nd, Sm, Eu) due to closing of charge-transfer gap. *Phys. Rev. B* **1992**, *45*, 8209–8212. [CrossRef]
8. Inaguma, Y.; Yoshida, M.; Tsuchiya, T.; Aimi, A.; Tanaka, K.; Katsumata, T.; Mori, D. High-pressure synthesis of novel lithium niobate-type oxides. *J. Phys. Conf. Ser.* **2010**, *215*, 012131. [CrossRef]
9. Ishiwata, S.; Azuma, M.; Takano, M.; Nishibori, E.; Takata, M.; Sakata, M.; Kato, K. High pressure synthesis, crystal structure and physical properties of a new Ni(ii) perovskite $BiNiO_3$. *J. Mater. Chem.* **2002**, *12*, 3733–3737. [CrossRef]

10. Inaguma, Y.; Katsumata, T. High Pressure Synthesis, Lattice Distortion, and Dielectric Properties of a Perovskite $Bi(Ni1/_2Ti1/_2)O_3$. *Ferroelectrics* **2003**, *286*, 111–117. [CrossRef]
11. Demazeau, G.; Marbeuf, A.; Pouchard, M.; Hagenmuller, P. Sur une série de composés oxygènes du nickel trivalent derivés de la perovskite. *J. Solid State Chem.* **1971**, *3*, 582–589. [CrossRef]
12. Alonso, J.A.; Martínez-Lope, M.J.; Casais, M.T.; Aranda, M.A.G.; Fernández-Díaz, M.T. Metal−Insulator Transitions, Structural and Microstructural Evolution of $RNiO_3$ (R = Sm, Eu, Gd, Dy, Ho, Y) Perovskites: Evidence for Room-Temperature Charge Disproportionation in Monoclinic $HoNiO_3$ and $YNiO_3$. *J. Am. Chem. Soc.* **1999**, *121*, 4754–4762. [CrossRef]
13. Alonso, J.A.; García-Muñoz, J.L.; Fernández-Díaz, M.T.; Aranda, M.A.G.; Martínez-Lope, M.J.; Casais, M.T. Charge Disproportionation in $RNiO_3$ Perovskites: Simultaneous Metal-Insulator and Structural Transition in $YNiO_3$. *Phys. Rev. Lett.* **1999**, *82*, 3871–3874. [CrossRef]
14. Alonso, J.A.; Martínez-Lope, M.J.; Casais, M.T.; García-Muñoz, J.L.; Fernández-Díaz, M.T. Room-temperature monoclinic distortion due to charge disproportionation in $RNiO_3$ perovskites with small rare-earth cations (R = Ho, Y, Er, Tm, Yb, and Lu): A neutron diffraction study. *Phys. Rev. B* **2000**, *61*, 1756–1763. [CrossRef]
15. Alonso, J.A.; Martínez-Lope, M.J.; Casais, M.T.; García-Muñoz, J.L.; Fernández-Díaz, M.T.; Aranda, M.A.G. High-temperature structural evolution of $RNiO_3$ (R = Ho, Y, Er, Lu) perovskites: Charge disproportionation and electronic localization. *Phys. Rev. B* **2001**, *64*, 094102. [CrossRef]
16. Mazin, I.I.; Khomskii, D.I.; Lengsdorf, R.; Alonso, J.A.; Marshall, W.G.; Ibberson, R.M.; Podlesnyak, A.; Martínez-Lope, M.J.; Abd-Elmeguid, M.M. Charge Ordering as Alternative to Jahn-Teller Distortion. *Phys. Rev. Lett.* **2007**, *98*, 176406. [CrossRef]
17. Presniakov, I.; Baranov, A.; Demazeau, G.; Rusakov, V.; Sobolev, A.; Alonso, J.A.; Martínez-Lope, M.J.; Pokholok, K. Evidence through Mössbauer spectroscopy of two different states for 57Fe probe atoms in $RNiO_3$ perovskites with intermediate-size rare earths, R = Sm, Eu, Gd, Dy. *J. Phys. Condens. Matter* **2007**, *19*, 036201. [CrossRef]
18. Caytuero, A.; Micklitz, H.; Abd-Elmeguid, M.M.; Litterst, F.J.; Alonso, J.A.; Baggio-Saitovitch, E.M. Evidence for charge disproportionation in monoclinic $EuNiO_3$ from 57Fe Mössbauer spectroscopy. *Phys. Rev. B* **2007**, *76*, 193105. [CrossRef]
19. Alonso, J.A.; Martínez-Lope, M.J.; Demazeau, G.; Fernández-Díaz, M.T.; Presniakov, I.A.; Rusakov, V.S.; Gubaidulina, T.V.; Sobolev, A.V. On the evolution of the $DyNiO_3$ perovskite across the metal–insulator transition though neutron diffraction and Mössbauer spectroscopy studies. *Dalton Trans.* **2008**, *46*, 6584–6592. [CrossRef] [PubMed]
20. García-Muñoz, J.L.; Aranda, M.A.G.; Alonso, J.A.; Martínez-Lope, M.J. Structure and charge order in the antiferromagnetic band-insulating phase of $NdNiO_3$. *Phys. Rev. B* **2009**, *79*, 134432. [CrossRef]
21. Kumar, D.; Rajeev, K.P.; Alonso, J.A.; Martínez-Lope, M.J. Slow dynamics in hard condensed matter: A case study of the phase separating system $NdNiO_3$. *J. Phys. Condens. Matter* **2009**, *21*, 185402. [CrossRef]
22. Kumar, D.; Rajeev, K.P.; Alonso, J.A.; Martínez-Lope, M.J. Evidence of kinetically arrested supercooled phases in the perovskite oxide $NdNiO_3$. *J. Phys. Condens. Matter* **2009**, *21*, 485402. [CrossRef]
23. Muñoz, A.; Alonso, J.A.; Martínez-Lope, M.J.; Fernández-Díaz, M.T. On the magnetic structure of $DyNiO_3$. *J. Solid State Chem.* **2009**, *182*, 1982–1989. [CrossRef]
24. Staub, U.; García-Fernández, M.; Mulders, A.M.; Bodenthin, Y.; Martínez-Lope, M.J.; Alonso, J.A. Soft x-ray resonant magnetic powder diffraction on $PrNiO_3$. *J. Phys. Condens. Matter* **2007**, *19*, 092201. [CrossRef]
25. Medarde, M.; Dallera, C.; Grioni, M.; Delley, B.; Vernay, F.; Mesot, J.; Sikora, M.; Alonso, J.A.; Martínez-Lope, M.J. Charge disproportionation in $RNiO_3$ perovskites (R = rare earth) from high-resolution x-ray absorption spectroscopy. *Phys. Rev. B* **2009**, *80*, 245105. [CrossRef]
26. Bodenthin, Y.; Staub, U.; Piamonteze, C.; García-Fernández, M.; Martínez-Lope, M.J.; Alonso, J.A. Magnetic and electronic properties of $RNiO_3$ (R = Pr, Nd, Eu, Ho and Y) perovskites studied by resonant soft x-ray magnetic powder diffraction. *J. Phys. Condens. Matter* **2011**, *23*, 036002. [CrossRef]
27. Sánchez-Benítez, J.; Martínez-Lope, M.J.; Alonso, J.A.; García-Muñoz, J.L. Magnetic and structural features of the $NdNi_{1-x}Mn_xO_3$ perovskite series investigated by neutron diffraction. *J. Phys. Condens. Matter* **2011**, *23*, 226001. [CrossRef]
28. Alonso, J.A.; Martínez-Lope, M.J.; Presniakov, I.A.; Sobolev, A.V.; Rusakov, V.S.; Gapochka, A.M.; Demazeau, G.; Fernández-Díaz, M.T. Charge disproportionation in $RNiO_3$ (R = Tm, Yb) perovskites observed in situ by neutron diffraction and 57Fe probe Mössbauer spectroscopy. *Phys. Rev. B* **2013**, *87*, 184111. [CrossRef]
29. Ramos, A.Y.; Piamonteze, C.; Tolentino, H.C.N.; Souza-Neto, N.M.; Bunau, O.; Joly, Y.; Grenier, S.; Itié, J.-P.; Massa, N.E.; Alonso, J.A.; et al. Stability of Ni sites across the pressure-induced insulator-to-metal transition in $YNiO_3$. *Phys. Rev. B* **2012**, *85*, 045102. [CrossRef]
30. Kumar, D.; Rajeev, K.P.; Alonso, J.A.; Martínez-Lope, M.J. Spin-canted magnetism and decoupling of charge and spin ordering in $NdNiO_3$. *Phys. Rev. B* **2013**, *88*, 014410. [CrossRef]
31. Serrano-Sánchez, F.; Fauth, F.; Martínez, J.L.; Alonso, J.A. Experimental Observation of Monoclinic Distortion in the Insulating Regime of $SmNiO_3$ by Synchrotron X-ray Diffraction. *Inorg. Chem.* **2019**, *58*, 11828–11835. [CrossRef]
32. Rao, C.N.R.; Raveau, B. *Colossal Magnetoresistance and Other Related Properties in 3d Oxides*; World Scientific: Singapore, 1998; ISBN 9789810232764.
33. Zeng, Z.; Greenblatt, M.; Subramanian, M.A.; Croft, M. Large Low-Field Magnetoresistance in Perovskite-type $CaCu_3Mn_4O_{12}$ without Double Exchange. *Phys. Rev. Lett.* **1999**, *82*, 3164–3167. [CrossRef]

34. Sánchez-Benítez, J.; Prieto, C.; de Andrés, A.; Alonso, J.A.; Martínez-Lope, M.J.; Casais, M.T. Evidence of two different Mn states in $CaCu_3Mn_4O_{12}$ derivatives with colossal magnetoresistance. *Phys. Rev. B* **2004**, *70*, 024419. [CrossRef]
35. Chenavas, J.; Joubert, J.C.; Marezio, M.; Bochu, B. The synthesis and crystal structure of $CaCu_3Mn_4O_{12}$: A new ferromagnetic-perovskite-like compound. *J. Solid State Chem.* **1975**, *14*, 25–32. [CrossRef]
36. Sánchez-Benítez, J.; Alonso, J.A.; Martínez-Lope, M.J.; Casais, M.T.; Martínez, J.L.; de Andrés, A.; Fernández-Díaz, M.T. Preparation, Crystal and Magnetic Structure, and Magnetotransport Properties of the Double Perovskite Ca $Cu_{2.5}Mn_{4.5}O_{12}$. *Chem. Mater.* **2003**, *15*, 2193–2200. [CrossRef]
37. Sánchez-Benítez, J.; Alonso, J.A.; Falcón, H.; Martínez-Lope, M.J.; De Andrés, A.; Fernández-Díaz, M.T. Preparation under high pressures and neutron diffraction study of new ferromagnetic $RCu_3Mn_4O_{12}$ (R = Pr, Sm, Eu, Gd, Dy, Ho, Tm, Yb) perovskites. *J. Phys. Condens. Matter* **2005**, *17*, S3063–S3068. [CrossRef]
38. Sánchez-Benítez, J.; Martínez-Lope, M.J.; Alonso, J.A. Preparation at moderate pressures, crystal and magnetic structure and magnetotransport of the ferrimagnetic $CeCu_3Mn_4O_{12}$ perovskite. *J. Appl. Phys.* **2010**, *107*, 103904. [CrossRef]
39. Sánchez-Benítez, J.; Martínez-Lope, M.J.; Alonso, J.A. Magnetism, Magnetotransport and Magnetic Structure of $ThCu_3Mn_4O_{12}$, Prepared at Moderate Pressures. *Zeitschrift für Naturforschung B* **2008**, *63*, 655–660. [CrossRef]
40. Alonso, J.A.; Sánchez-Benítez, J.; De Andrés, A.; Martínez-Lope, M.J.; Casais, M.T.; Martínez, J.L. Enhanced magnetoresistance in the complex perovskite $LaCu_3Mn_4O_{12}$. *Appl. Phys. Lett.* **2003**, *83*, 2623–2625. [CrossRef]
41. Jahn-Teller Distortions. (2020, August 15). Available online: https://chem.libretexts.org/@go/page/519 (accessed on 8 April 2021).
42. Sánchez-Benítez, J.; Alonso, J.A.; de Andrés, A.; Martínez-Lope, M.J.; Martínez, J.L.; Muñoz, A. Peculiar Magnetic Behavior of the $ThCu_3Mn_4O_{12}$ Complex Perovskite. *Chem. Mater.* **2005**, *17*, 5070–5076. [CrossRef]
43. Sánchez-Benítez, J.; Alonso, J.A.; Martínez-Lope, M.J.; de Andrés, A.; Fernández-Díaz, M.T. Enhancement of the Curie Temperature along the Perovskite Series $RCu_3Mn_4O_{12}$ Driven by Chemical Pressure of R^{3+} Cations (R = Rare Earths). *Inorg. Chem.* **2010**, *49*, 5679–5685. [CrossRef]
44. de la Calle, C.; Sánchez-Benítez, J.; Barbanson, F.; Nemes, N.; Fernández-Díaz, M.T.; Alonso, J.A. Transition from Pauli-paramagnetism to ferromagnetism in $CaCu_3(Ru_{4-x}Mn_x)O_{12}$ ($0 \leq x \leq 3$) perovskites. *J. Appl. Phys.* **2011**, *109*, 123914. [CrossRef]
45. Subramanian, M.A.; Ramirez, A.P.; Marshall, W.J. Structural Tuning of Ferromagnetism in a 3D Cuprate Perovskite. *Phys. Rev. Lett.* **1999**, *82*, 1558–1561. [CrossRef]
46. Kimura, T.; Kawamoto, S.; Yamada, I.; Azuma, M.; Takano, M.; Tokura, Y. Magnetocapacitance effect in multiferroic $BiMnO_3$. *Phys. Rev. B* **2003**, *67*, 180401. [CrossRef]
47. Belik, A.A.; Yokosawa, T.; Kimoto, K.; Matsui, Y.; Takayama-Muromachi, E. High-Pressure Synthesis and Properties of Solid Solutions between $BiMnO_3$ and $BiScO_3$. *Chem. Mater.* **2007**, *19*, 1679–1689. [CrossRef]
48. Toulemonde, P.; Darie, C.; Goujon, C.; Legendre, M.; Mendonca, T.; Álvarez-Murga, M.; Simonet, V.; Bordet, P.; Bouvier, P.; Kreisel, J.; et al. Single crystal growth of $BiMnO_3$ under high pressure–high temperature. *High Press. Res.* **2009**, *29*, 600–604. [CrossRef]
49. Montanari, E.; Righi, L.; Calestani, G.; Migliori, A.; Gilioli, E.; Bolzoni, F. Room Temperature Polymorphism in Metastable $BiMnO_3$ Prepared by High-Pressure Synthesis. *Chem. Mater.* **2005**, *17*, 1765–1773. [CrossRef]
50. Goodenough, J.B. *Magnetism and the Chemical Bond*; Interscience-Wiley: New York, NY, USA, 1963.
51. Muñoz, A.; Alonso, J.A.; Martínez-Lope, M.J.; Morán, E.; Escamilla, R. Synthesis and study of the crystallographic and magnetic structure of $SeCoO_3$. *Phys. Rev. B* **2006**, *73*, 104442. [CrossRef]
52. Muñoz, A.; Alonso, J.A.; Martínez-Lope, M.J.; Falcón, H.; García-Hernández, M.; Morán, E. High-pressure synthesis and study of the crystal and magnetic structure of the distorted $SeNiO_3$ and $SeMnO_3$ perovskites. *Dalton Trans.* **2006**, *41*, 4936–4943. [CrossRef]
53. Martínez-Lope, M.J.; Retuerto, M.; Alonso, J.A.; Sánchez-Benítez, J.; Fernández-Díaz, M.T. High-pressure synthesis and neutron diffraction investigation of the crystallographic and magnetic structure of $TeNiO_3$ perovskite. *Dalton Trans.* **2011**, *40*, 4599. [CrossRef]
54. Ridley, C.J.; Knight, K.S.; Wilson, C.W.; Smith, R.I.; Bull, C.L. Structure and physical properties of $SeCo_{1-x}Mn_xO_3$. *J. Phys. Condens. Matter* **2019**, *31*, 395402. [CrossRef] [PubMed]
55. Cabuk, S. Magnetic, electronic and mechanical properties of $SeXO_3$ (X = Mn, Ni) with the LSDA + U framework. *J. Alloys Compd.* **2021**, *850*, 156674. [CrossRef]
56. Liang, G.; Huot, J.; Schulz, R. Hydrogen storage properties of the mechanically alloyed $LaNi_5$-based materials. *J. Alloys Compd.* **2001**, *320*, 133–139. [CrossRef]
57. Retuerto, M.; Sánchez-Benítez, J.; Alonso, J.A.; Leardini, F.; Ares, J.R.; Fernández, J.F.; Sánchez, C. Deuteration properties of $CaNi_{5-x}Cu_x$ system. *J. Power Sources* **2011**, *196*, 4342–4346. [CrossRef]
58. Martínez-Coronado, R.; Retuerto, M.; Torres, B.; Martínez-Lope, M.J.; Fernández-Díaz, M.T.; Alonso, J.A. High-pressure synthesis, crystal structure and cyclability of the Mg_2NiH_4 hydride. *Int. J. Hydrogen Energy* **2013**, *38*, 5738–5745. [CrossRef]
59. Martínez-Coronado, R.; Sánchez-Benítez, J.; Retuerto, M.; Fernández-Díaz, M.T.; Alonso, J.A. High-pressure synthesis of Na1−xLixMgH3 perovskite hydrides. *J. Alloys Compd.* **2012**, *522*, 101–105. [CrossRef]
60. Andrada-Chacón, A.; Alonso, J.A.; Pomjakushin, V.; Sánchez-Benítez, J. High-pressure synthesis and structural characterization of Na1-K MgH_3 perovskite hydrides. *J. Alloys Compd.* **2017**, *729*, 914–920. [CrossRef]
61. Shimakawa, Y.; Kubo, Y.; Manako, T. Giant magnetoresistance in $Ti_2Mn_2O_7$ with the pyrochlore structure. *Nature* **1996**, *379*, 53–55. [CrossRef]

62. Subramanian, M.A.; Toby, B.H.; Ramirez, A.P.; Marshall, W.J.; Sleight, A.W.; Kwei, G.H. Colossal Magnetoresistance Without Mn^{3+}/Mn^{4+} Double Exchange in the Stoichiometric Pyrochlore $Tl_2Mn_2O_7$. *Science* **1996**, *273*, 81–84. [CrossRef]
63. Shimakawa, Y.; Kubo, Y.; Hamada, N.; Jorgensen, J.D.; Hu, Z.; Short, S.; Nohara, M.; Takagi, H. Crystal structure, magnetic and transport properties, and electronic band structure of $A_2Mn_2O_7$ pyrochlores (A = Y, In, Lu and Tl). *Phys. Rev. B* **1999**, *59*, 1249–1254. [CrossRef]
64. Núñez-Regueiro, M.D.; Lacroix, C. Origin and pressure dependence of ferromagnetism in $A_2Mn_2O_7$ pyrochlores (A = Y, In, Lu and Tl). *Phys. Rev. B* **2000**, *63*, 014417. [CrossRef]
65. Alonso, J.A.; Martínez, J.L.; Martínez-Lope, M.J.; Casais, M.T.; Fernández-Díaz, M.T. Room Temperature Magnetoresistance and Cluster-Glass Behavior in the $Tl_{2-x}BixMn_2O_7$ ($0 \leq x \leq 0.5$) pyrochlore series. *Phys. Rev. Lett.* **1999**, *82*, 189–192. [CrossRef]
66. Alonso, J.A.; Velasco, P.; Martínez-Lope, M.J.; Casais, M.T.; Martínez, J.L.; Fernández-Díaz, M.T.; de Paoli, J.M. Unprecedented magnetoresistance in Cd-substituted $Tl_2Mn_2O_7$ pyrochlores. *Appl. Phys. Lett.* **2000**, *76*, 3274–3276. [CrossRef]
67. Alonso, J.A.; Martínez-Lope, M.J.; Casais, M.T.; Velasco, P.; Martínez, J.L.; Fernández-Díaz, M.T.; de Paoli, J.M. Enhancement of ferromagnetic coupling in Sb-substituted $Tl_2Mn_2O_7$ pyrochlores. *Phys. Rev. B* **1999**, *60*, R15024–R15027. [CrossRef]
68. Alonso, J.A.; Martínez-Lope, M.J.; Casais, M.T.; Martínez, J.L.; Fernández-Díaz, M.T. Large Increase in Magnetoresistance and Cluster-Glass Behavior in Defect $Tl_{2-x}Mn_2O_{7-y}$ Pyrochlores. *Chem. Mater.* **2000**, *12*, 1127–1133. [CrossRef]
69. Velasco, P.; Alonso, J.A.; Tissen, V.G.; Marshall, W.G.; Casais, M.T.; Martínez-Lope, M.J.; de Andrés, A.; Prieto, C.; Martínez, J.L. Pressure effect in the structure, transport properties, and magnetic interactions of $Tl_2Mn_2O_7$ pyrochlores derivatives. *Phys. Rev. B* **2003**, *67*, 104403. [CrossRef]
70. Li, J.-F.; Liu, W.-S.; Zhao, L.-D.; Zhou, M. High-performance nanostructured thermoelectric materials. *NPG Asia Mater.* **2010**, *2*, 152–158. [CrossRef]
71. Snyder, G.J.; Toberer, E.S. Complex thermoelectric materials. *Nat. Mater.* **2008**, *7*, 105–114. [CrossRef]
72. Nolas, G.S.; Morelli, D.T.; Tritt, T.M. SKUTTERUDITES: A Phonon-Glass-Electron Crystal Approach to Advanced Thermoelectric Energy Conversion Applications. *Annu. Rev. Mater. Sci.* **1999**, *29*, 89–116. [CrossRef]
73. Serrano, F.; Gharsallah, M.; Cherif, W.; Martínez, J.L.; Cascos, V.; Troncoso, L.; Alonso, J.A. Facile Preparation of State-of-the Art Thermoelectric Materials by High-pressure Synthesis. *Mater. Today Proc.* **2015**, *2*, 661–668. [CrossRef]
74. Li, X.; Zhang, Q.; Kang, Y.; Chen, C.; Zhang, L.; Yu, D.; Tian, Y.; Xu, B. High pressure synthesized Ca-filled $CoSb_3$ skutterudites with enhanced thermoelectric properties. *J. Alloys Compd.* **2016**, *677*, 61–65. [CrossRef]
75. Kang, Y.; Yu, F.; Chen, C.; Zhang, Q.; Sun, H.; Zhang, L.; Yu, D.; Tian, Y.; Xu, B. High pressure synthesis and thermoelectric properties of Ba-filled $CoSb_3$ skutterudites. *J. Mater. Sci. Mater. Electron.* **2017**, *28*, 8771–8776. [CrossRef]
76. Yang, J.; Zhang, L.; Liu, Y.; Chen, C.; Li, J.; Yu, D.; He, J.; Liu, Z.; Tian, Y.; Xu, B. Investigation of skutterudite $MgyCo_4Sb_{12}$: High pressure synthesis and thermoelectric properties. *J. Appl. Phys.* **2013**, *113*, 113703. [CrossRef]
77. Slack, G.A. *CRC Handbook of Thermoelectrics*; Rowe, D.M., Ed.; CRC Press: Boca Raton, FL, USA, 1995; ISBN 0849301467.
78. Rull-Bravo, M.; Moure, A.; Fernández, J.F.; Martín-González, M. Skutterudites as thermoelectric materials: Revisited. *RSC Adv.* **2015**, *5*, 41653–41667. [CrossRef]
79. Liu, Z.-Y.; Zhu, J.-L.; Tong, X.; Niu, S.; Zhao, W.-Y. A review of $CoSb_3$-based skutterudite thermoelectric materials. *J. Adv. Ceram.* **2020**, *9*. [CrossRef]
80. Prado-Gonjal, J.; Serrano-Sánchez, F.; Nemes, N.M.; Dura, O.J.; Martínez, J.L.; Fernández-Díaz, M.T.; Fauth, F.; Alonso, J.A. Extra-low thermal conductivity in unfilled $CoSb_3$-δskutterudite synthesized under high-pressure conditions. *Appl. Phys. Lett.* **2017**, *111*, 1–6. [CrossRef]
81. Serrano-Sánchez, F.; Prado-Gonjal, J.; Nemes, N.M.; Biskup, N.; Varela, M.; Dura, O.J.; Martínez, J.L.; Fernández-Díaz, M.T.; Fauth, F.; Alonso, J.A. Low thermal conductivity in La-filled cobalt antimonide skutterudites with an inhomogeneous filling factor prepared under high-pressure conditions. *J. Mater. Chem. A* **2017**, *6*, 118–126. [CrossRef]
82. Serrano-Sánchez, F.; Prado-Gonjal, J.; Nemes, N.M.; Biskup, N.; Dura, O.J.; Martínez, J.L.; Fernández-Díaz, M.T.; Fauth, F.; Alonso, J.A. Thermal Conductivity Reduction by Fluctuation of the Filling Fraction in Filled Cobalt Antimonide Skutterudite Thermoelectrics. *ACS Appl. Energy Mater.* **2018**, *1*, 6181–6189. [CrossRef]
83. Gainza, J.; Serrano-Sánchez, F.; Prado-Gonjal, J.; Nemes, N.M.; Biskup, N.; Dura, O.J.; Martínez, J.L.; Fauth, F.; Alonso, J.A. Substantial thermal conductivity reduction in mischmetal skutterudites $Mm_xCo_4Sb_{12}$ prepared under high-pressure conditions, due to uneven distribution of the rare-earth elements. *J. Mater. Chem. C* **2019**, *7*, 4124–4131. [CrossRef]
84. Takizawa, H.; Okazaki, K.; Uheda, K.; Endo, T.; Nolas, G.S. High Pressure Synthesis of New Filled Skutterudites. *MRS Proc.* **2001**, *691*, G2.3. [CrossRef]
85. Liu, Y.; Li, X.; Zhang, Q.; Zhang, L.; Yu, D.; Xu, B.; Tian, Y. High Pressure Synthesis of p-Type $CeyFe_{4-x}Co_xSb_{12}$ Skutterudites. *Materials* **2016**, *9*, 257. [CrossRef] [PubMed]
86. Zhao, P.; Sun, H.; Yu, F.; Wang, B.; Zhao, H.; Wang, D.; Yu, D.; Tian, Y.; Xu, B. Thermoelectric performance of p-type $CaFe_{1.3}Co_{2.7}Sb_{12}$ skutterudites from high pressure synthesis. *J. Alloys Compd.* **2021**, *851*, 156928. [CrossRef]
87. Zhang, J.; Xu, B.; Wang, L.-M.; Yu, D.; Yang, J.; Yu, F.; Liu, Z.; He, J.; Wen, B.; Tian, Y. High-pressure synthesis of phonon-glass electron-crystal featured thermoelectric $LixCo_4Sb_{12}$. *Acta Mater.* **2012**, *60*, 1246–1251. [CrossRef]
88. Chen, C.; Zhang, L.; Li, J.; Yu, F.; Yu, D.; Tian, Y.; Xu, B. Enhanced thermoelectric performance of lanthanum filled $CoSb_3$ synthesized under high pressure. *J. Alloys Compd.* **2017**, *699*, 751–755. [CrossRef]

89. Ren, W.; Geng, H.; Zhang, Z.; Zhang, L. Filling-Fraction Fluctuation Leading to Glasslike Ultralow Thermal Conductivity in Caged Skutterudites. *Phys. Rev. Lett.* **2017**, *118*, 1–6. [CrossRef] [PubMed]
90. Gainza, J.; Serrano-Sánchez, F.; Rodrigues, J.E.; Prado-Gonjal, J.; Nemes, N.M.; Biskup, N.; Dura, O.J.; Martínez, J.L.; Fauth, F.; Alonso, J.A. Unveiling the Correlation between the Crystalline Structure of M-Filled $CoSb_3$ (M = Y, K, Sr) Skutterudites and Their Thermoelectric Transport Properties. *Adv. Funct. Mater.* **2020**, *30*, 2001651. [CrossRef]